

Supplementary material

**Data-based estimates of interannual sea–air CO₂ flux variations
1957–2020 and their relation to environmental drivers**

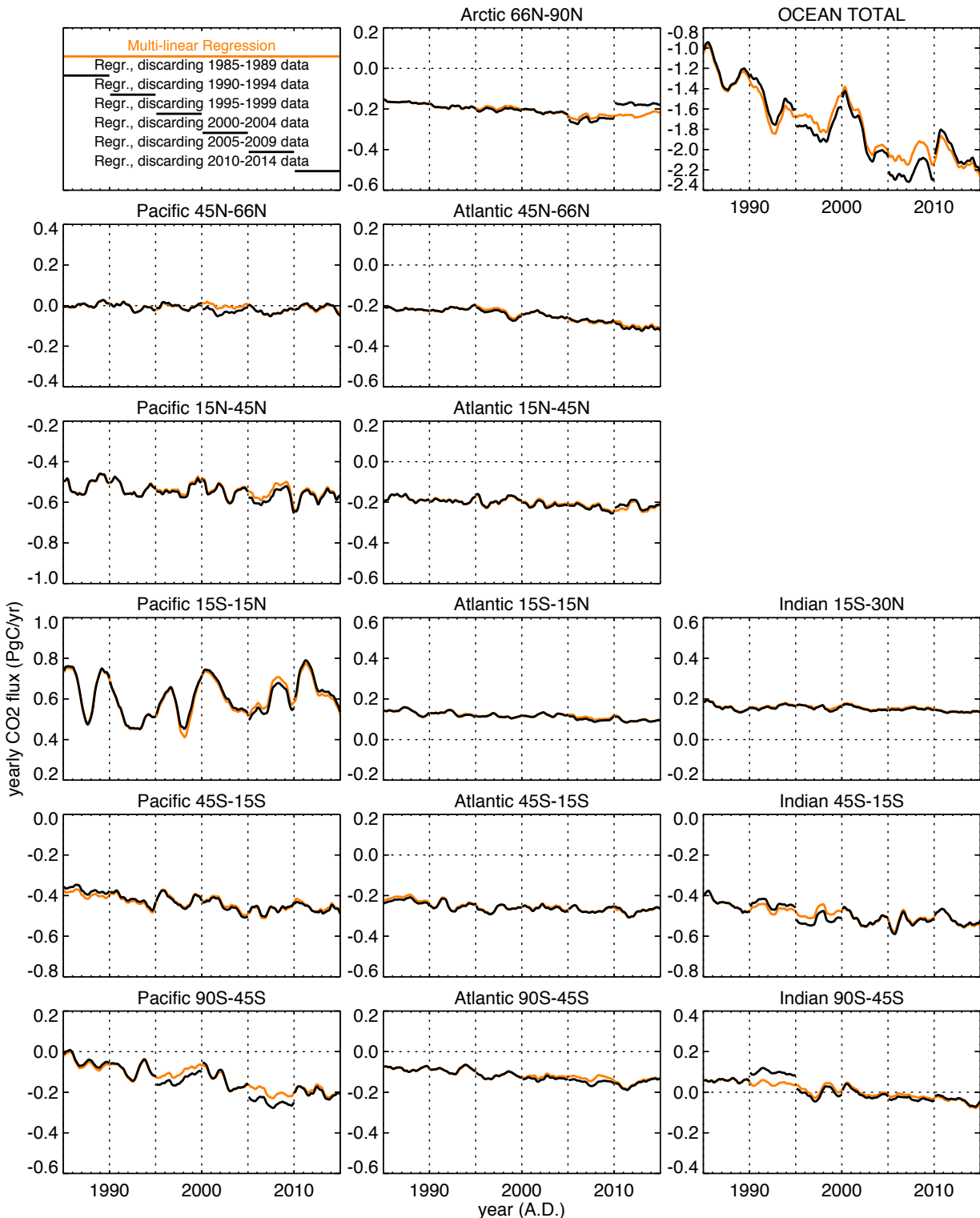


Figure S1. Predictive skill of the regression:

Interannual variations of the sea–air CO₂ flux estimated by the multi-linear regression using all $p\text{CO}_2$ data (orange) and by test regressions with artificial 5-year data gaps (Sect. 2.2, black) as in the example in Fig. 5 (middle). For clarity, the test runs are only shown during their respective data gaps, i.e., the reconstructed flux variations only.

The figure demonstrates that the predictive skill illustrated in Fig. 5 (middle) holds generally for all parts of the ocean and other 5-year data gaps. In some cases (especially in regions south of 45° S), the long-term mean cannot completely be reconstructed without the respective discarded data, but the year-to-year variability mostly stays the same. This means that no particular $p\text{CO}_2$ data point is causing features in the flux variability and the sensitivities γ_i estimated by the multi-linear regression by its own.

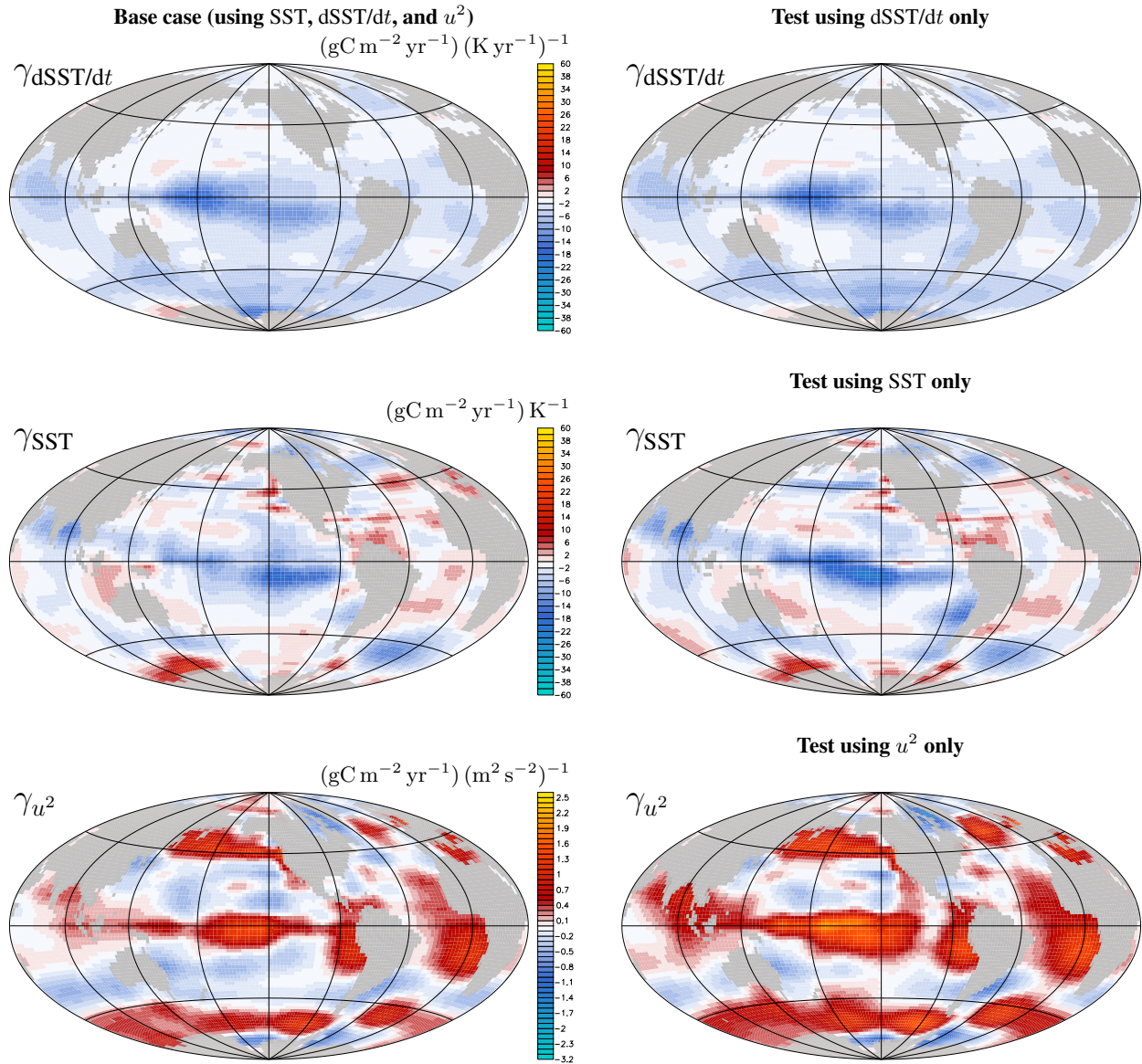


Figure S2. Testing the mutual independence of the explanatory variables in the regression:

Estimated sensitivities of the internal DIC flux against non-seasonal variations in SST, dSST/dt, and u^2 . *Left:* Base case (using all of SST, dSST/dt, and u^2) as in Fig. 7. *Right:* Three test regressions each using the respective one of the explanatory variables only.

The sensitivity patterns from the three test regressions using individual explanatory variables (right) are similar to the base case using all three together (left), especially for the sensitivity against dSST/dt (top row). This could not be the case if there would be substantial collinearity between the explanatory variables. We conclude that the sensitivities can be estimated rather independently from each other. The sensitivities against SST (middle) and u^2 (bottom), when used individually, are slightly increased, which may indicate a small amount of collinearity between these two.

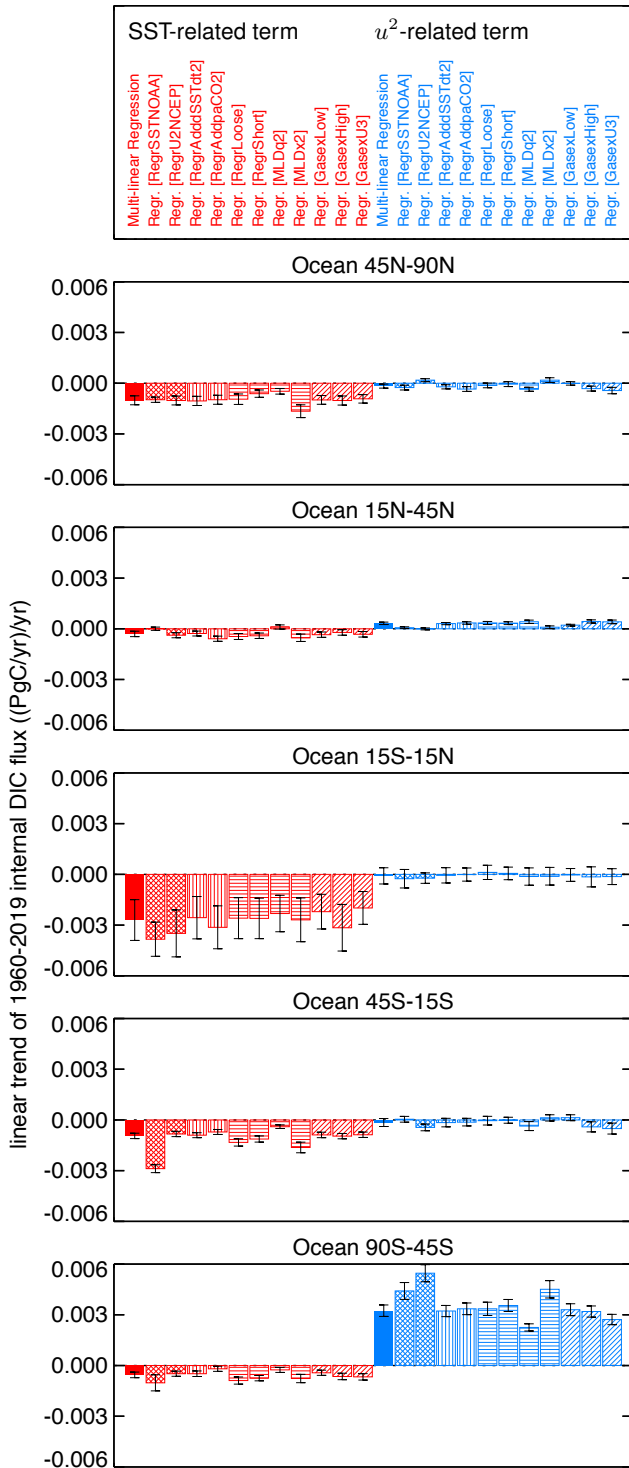


Figure S3. Contributions to the secular carbon flux trend:

Linear 1960–2019 trends of the regression terms related to SST (red) and u^2 (light blue) from Fig. 6 (base case of the multi-linear regression, solid bars) and various uncertainty cases (Table 2, hashed bars). The trends in the regression terms (contributions to the ocean-internal DIC flux) cause contributions to the trends in sea–air CO₂ flux of very similar strength (not shown). The error bars give the formal error of the slope calculated from 5-year flux averages as in Fig. 10. The uncertainty case *RegrNoDecad* has been omitted here because it artificially lacks any trends in SST and u^2 by construction. The uncertainty case *RegrAddU4* has been omitted as well because a large part of the wind-related trend is contained in the additional u^4 regression term and would thus be invisible here. The regression term related to $dSST/dt$ is not shown because it has very small trends (see Fig. 6).

*The rising SST causes some trend towards less CO₂ source in the tropics (mainly in the tropical Pacific) due to the negative γ_{SST} sensitivities estimated there (Fig. 7, middle). Some smaller trends are also found in the other latitudinal bands. The estimated trend gets more negative when using SST data from NOAA-ER (*RegrSSTNOAA*) rather than Hadley EN, which is related to a jump in SST values in the NOAA-ER reconstruction. Also the use of wind speed data from NCEP (*RegrU2NCEP*) changes the estimated trend, pointing to some statistical dependence between the regression terms related to SST and u^2 . We are not confident that the estimated SST-related trend reflects a real mechanism, but rather assume that the response of f_{int} to a secular temperature trend is not well described by the γ_{SST} sensitivities determined in the regression by variability on the ENSO time scale. For example, ENSO-related SST variations originate from changes in upwelling which also affects carbon fluxes, while the secular SST trend is rather caused by heat uptake from the atmosphere.*

*Wind-related trends are small in all latitudinal bands except for the Southern Ocean, where the secular increase in wind speeds leads to more and more CO₂ outgassing. When using NCEP wind speed data (*RegrU2NCEP*), the estimated trend is larger than in the base case using JRA55-do wind speeds. Again, we also see some cross effect when using the alternative SST data set (*RegrSSTNOAA*). The trend estimate in the Southern Ocean is further affected by mixed-layer depth (MLDq2, MLDx2).*

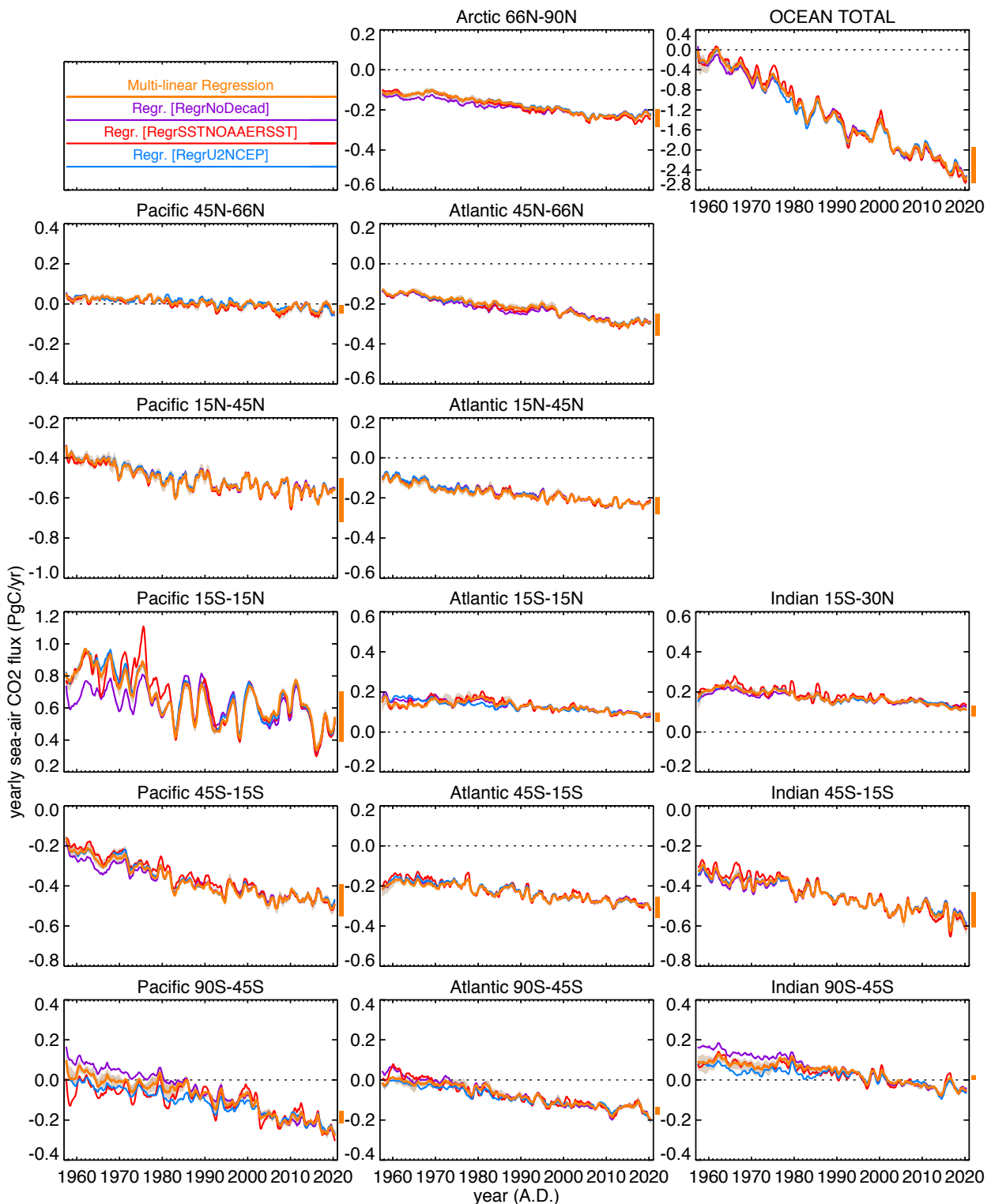


Figure S4. Results of the uncertainty cases:

Yearly sea–air CO₂ flux as in Fig. 3 estimated by the multi-linear regression (base case, orange) and the uncertainty cases listed in Sect. 2.1.4. The cases with the largest impact on interannual variability (RegrSSTNOAA, RegrU2NCEP, RegrAddpaCO2, RegrNoDecad) are plotted explicitly in different colors. As the cases related to gas exchange (GasexLow, GasexHigh, GasexU3) shift the long-term mean of the flux, the range of this shift has been indicated by the length of the vertical orange bars just outside each panel for clarity. Due to their rather small impact, the remaining uncertainty cases (RegrAddSSTdt2, RegrAddU4, RegrLoose, RegrShort, MLDq2, MLDx2) have been subsumed into the pale orange band depicting their envelope.

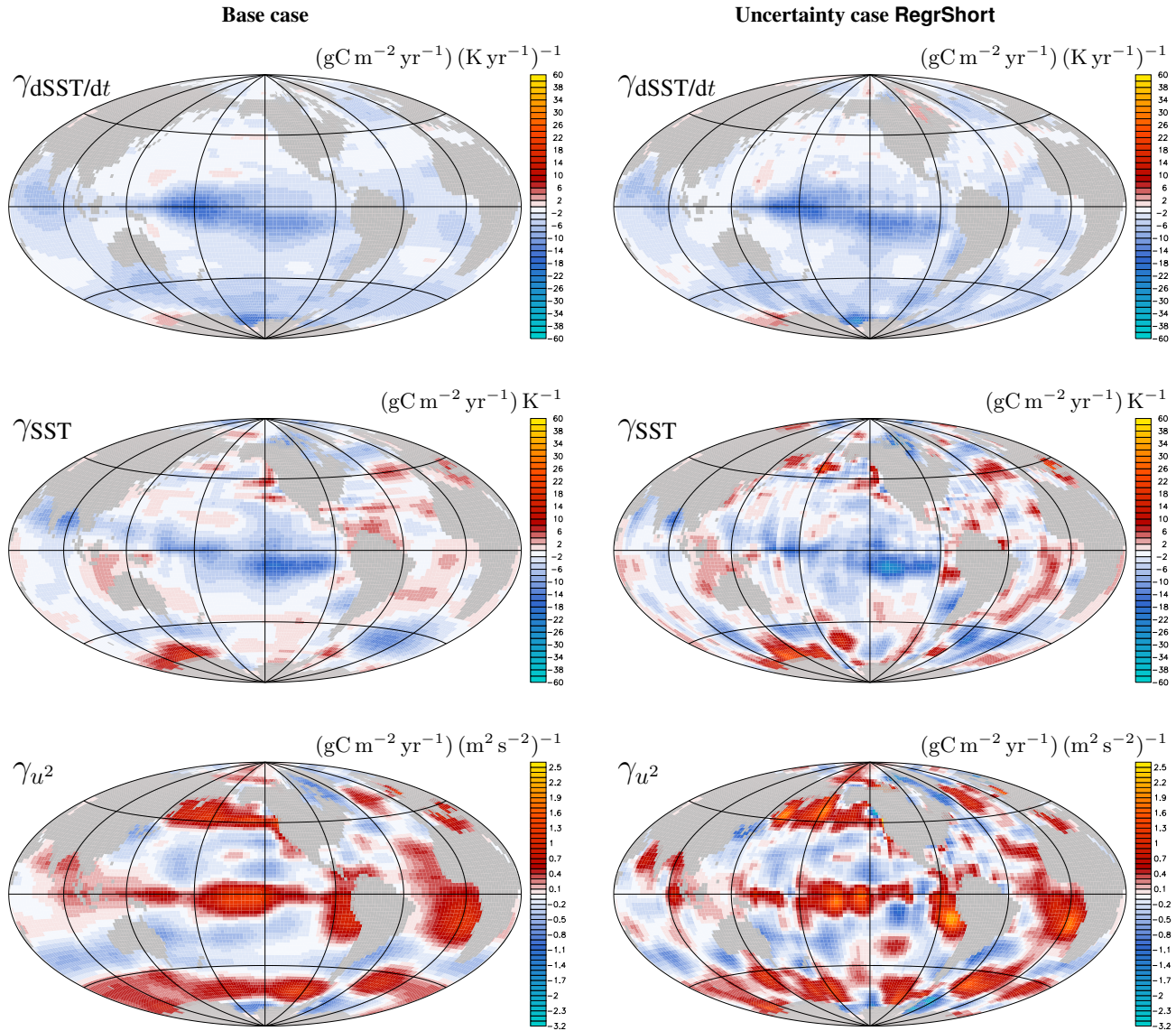


Figure S5. Impact of the chosen a-priori correlation lengths:

Sensitivities of f_{int} to changes in the explanatory variables as in Fig. 7 estimated by the base case (left, identical to Fig. 7) and by the uncertainty case RegrShort with a shorter a-priori correlation length scales in the 3 regression terms where any decadal variability from the 3 explanatory variables has been removed (right).

Even though the flux variability hardly changes when using shorter a-priori correlation lengths for adjusting the sensitivities (RegrShort being part of the narrow uncertainty band in Fig. S4), the spatial patterns of the underlying sensitivities (γ_i) notably become more patchy, especially for γ_{SST} (middle right) and γ_{u^2} (bottom right). As best seen in the wind speed sensitivity (bottom), the patches sometimes align with areas of temporally more dense data constraints, for example at the locations of the Tropical Atmosphere Ocean (TAO) mooring array along the Equator in the Pacific. Clearly, patterns resembling the density of observation are unlikely to be true. As the actual sensitivities estimated for these “data hotspots” are quite similar across these locations (and as the regionally integrated fluxes do not change much either), spreading out the sensitivities into the intermediate areas by the longer correlations, as done in our base case, seems to be justified and more appropriate.

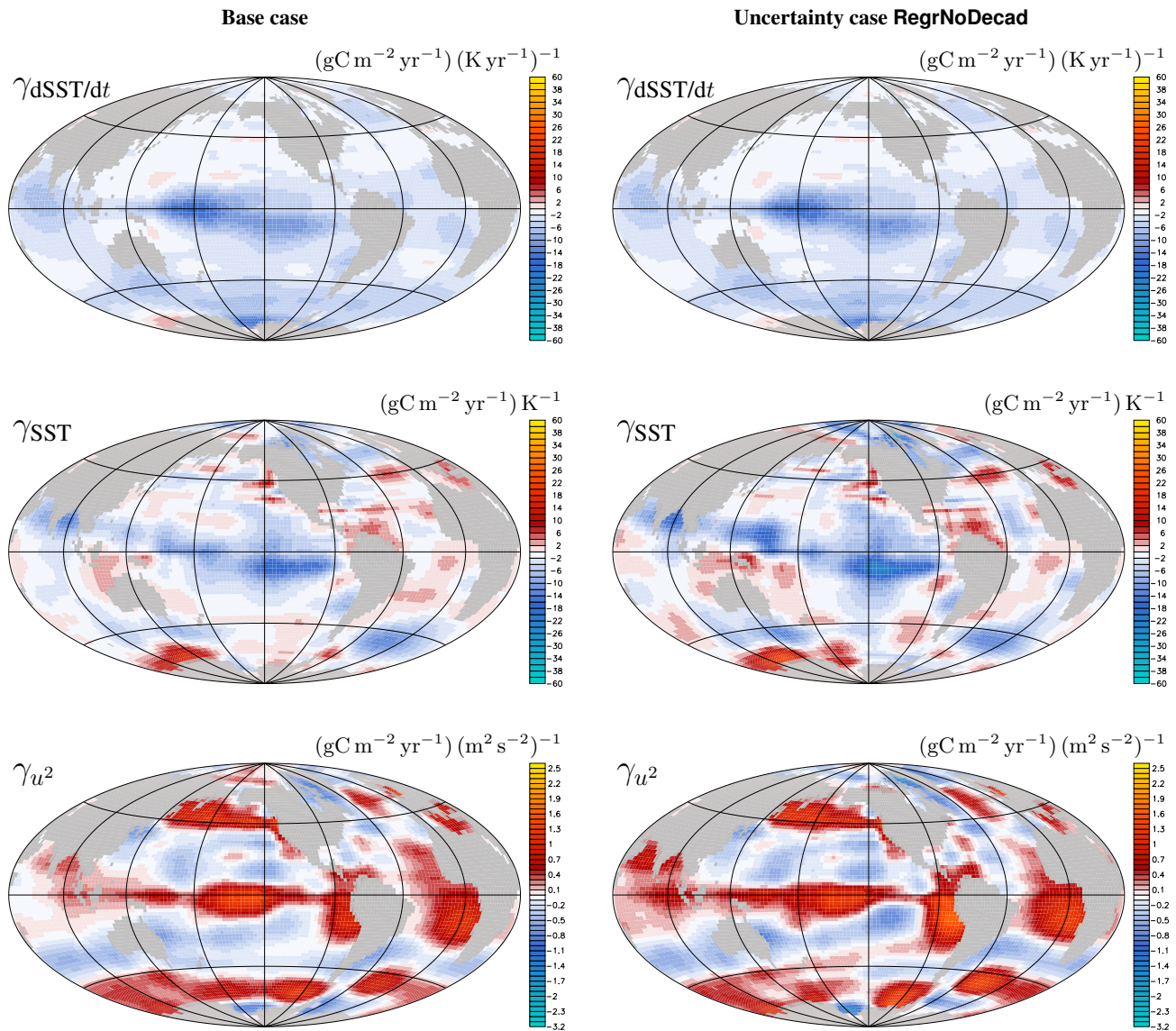


Figure S6. Impact of secular trends in the explanatory variables:

Sensitivities of f_{int} to changes in the explanatory variables as in Fig. 7 estimated by the base case (left, identical to Fig. 7) and by the uncertainty case ReGrNoDecad where any decadal variability (including any secular trend) has been removed from the 3 explanatory variables (right).

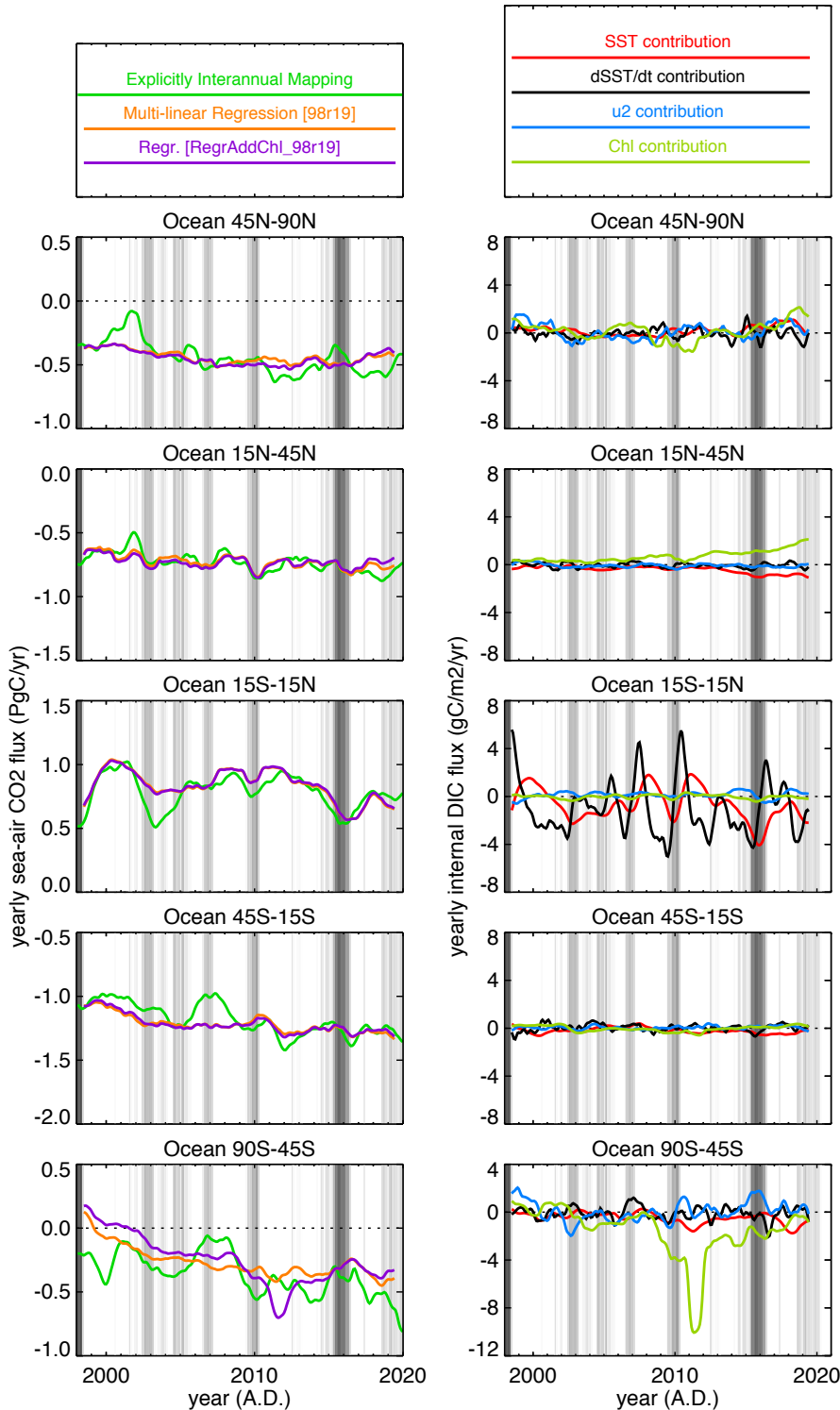


Figure S7. Using chlorophyll concentration as additional explanatory variable:

Left: Interannual variations of the sea–air CO₂ flux estimated by the explicitly interannual mapping (green), a multi-linear regression with the base set of explanatory variables (orange), and a regression using chlorophyll-a concentration from the GlobColour project (Maritorena et al., 2010) as additional explanatory variable (run `RegrAddChl_98r19`, magenta). Both regression runs are done over the period 1998–2019 only when chlorophyll-a data are available. *Right:* For the test regression involving chlorophyll-a concentration, contributions of the various explanatory variables to the interannual variations of the ocean-internal DIC sources/sinks as in Fig. 6.

The addition of chlorophyll concentration as explanatory variable is seen to cause only small changes in the total interannual variations (magenta vs. orange, left). The largest deviations occur in the Southern Ocean (bottom), but they do not obviously increase the similarity with the explicitly interannual estimate (green).

Correspondingly, the contributions from the chlorophyll regression term are mostly small compared to the other contributions (right). The most prominent feature of the chlorophyll contribution is a large spike in the Southern Ocean in early 2011, from a corresponding spike in the chlorophyll data set. It translates into a notable reduction in the sea–air CO₂ flux (bottom left). We assume the spike to be an artifact in the chlorophyll data set.

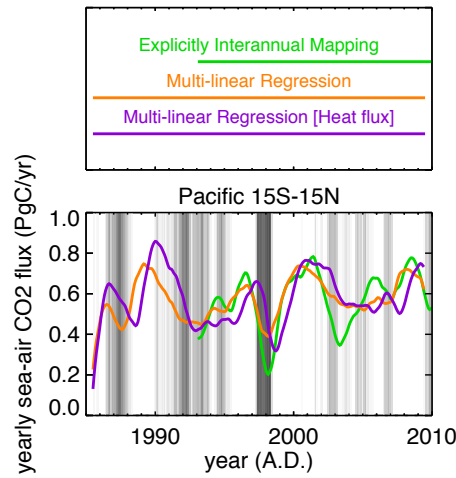


Figure S8. Using heat flux as alternative explanatory variable:

Interannual sea–air CO₂ flux variations estimated by the explicitly interannual estimation (green), the multi-linear regression (here only regressing over 1985–2009, orange), and the multi-linear regression using heat flux (taken from the OAFlux project Yu and Weller, 2007) as explanatory variable instead of dSST/dt (run RegrHeat_85r09, magenta).

We tested heat flux as an alternative explanatory variable replacing dSST/dt because heat flux is related to the amount of exchange between the mixed layer and deeper water. However, without dSST/dt the multi-linear regression is not able to represent the timing of El Niño events in the tropical Pacific correctly. This is consistent with the dominance of the dSST/dt regression term in the tropical Pacific (Fig. 6), which has a temporal pattern quite different from that of heat flux. In the other regions, heat flux does not seem to pick up interannual signals from the pCO₂ data either.

The spatial pattern of the heat flux sensitivity is markedly different from that of dSST/dt. In particular, it is more patchy and comprises both positive and negative sign (Fig. S9 below).

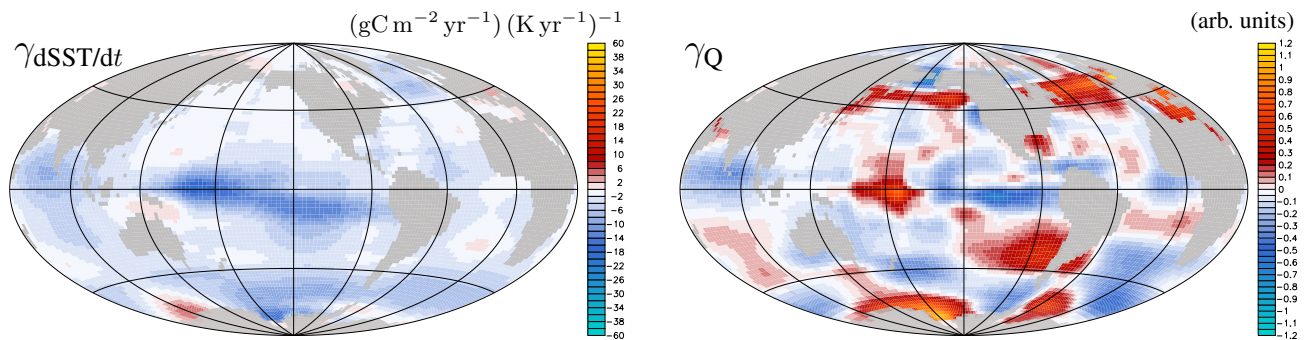


Figure S9. Left: Sensitivity of f_{int} to changes in dSST/dt estimated by the base case (as Fig. 7, but regression only run over 1985–2009 to be consistent with heat flux case as in Fig. S8); **Right:** Sensitivity of f_{int} to changes in heat flux (Q), estimated by a test case replacing dSST/dt by heat flux as one of the explanatory variables (heat flux is only available over 1985–2009).

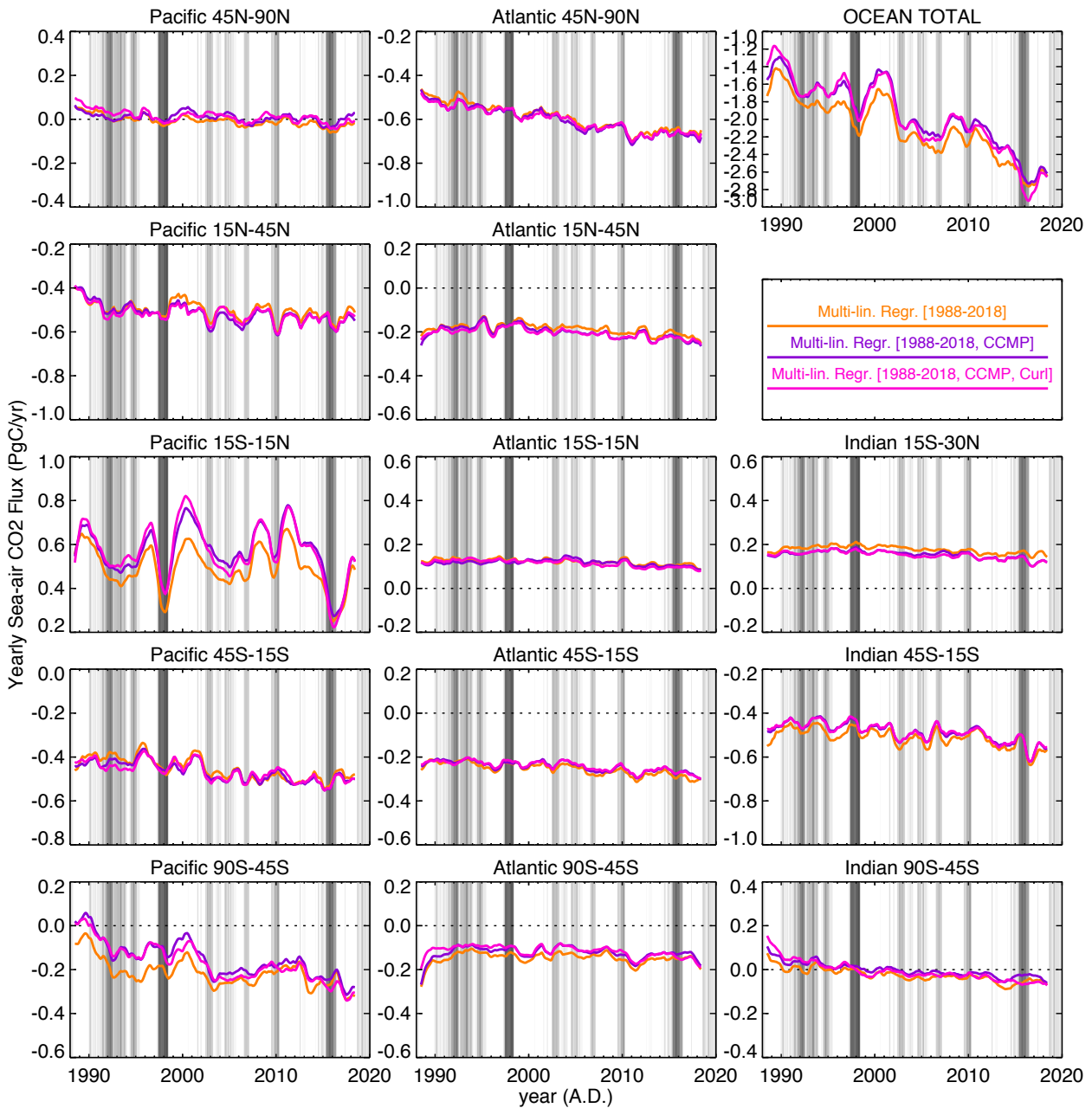


Figure S10. Interannual variations of the sea–air CO₂ flux estimated by an multi-linear regression using NCEP-based squared wind speeds as in the base case (orange), using CCMP-based squared wind speeds (violet), and wind stress curl calculated from CCMP wind speeds (magenta). All regressions have been done over 1988–2018 only.

Wind stress curl may be a better predictor for ocean-internal DIC sources and sinks than squared wind speed, because it is related to Ekman pumping/suction. We therefore also tried replacing squared wind speed by wind stress curl. For the technical reason of its finer resolution, we used gridded wind data from CCMP v2.0 (Cross-Calibrated Multi-Platform, Atlas et al., 2011) to calculate the wind stress curl. This gives us the additional opportunity to test the uncertainty inherited from the wind speed data set. Unfortunately, CCMP wind speeds are only available over 1988–2018.

In some regions, the interannual variations of the sea–air CO₂ flux changes notably when replacing NCEP winds by CCMP winds (orange vs. violet). This very likely reflects the influence of the wind speed product on gas exchange. In contrast, the CO₂ flux variations calculated from squared wind speed or the wind stress curl (violet vs. magenta) are not much different. However, the spatial pattern of the sensitivity against wind stress curl is more patchy than the sensitivity against squared wind speed (not shown). This is probably related to the fact that the wind stress curl can have both positive and negative sign, while the squared wind speed is always positive.